Analysis of the optical feedback dynamics in InAs/GaAs quantum dot lasers directly grown on silicon

HEMING HUANG,[1,*] JIANAN DUAN,[1] DAEHWAN JUNG,[2] ALAN Y. LIU,[3] ZEYU ZHANG,[4] JUSTIN NORMAN,[4] JOHN E. BOWERS,[3,4] AND FRÉDÉRIC GRILLOT[1,5]

[1]*LTCI, Télécom ParisTech, Université Paris-Saclay, 46 rue Barrault, 75013 Paris, France*
[2]*Institute for Energy Efficiency, University of California Santa Barbara, Santa Barbara, California 93106, USA*
[3]*Materials Department, University of California Santa Barbara, Santa Barbara, California 93106, USA*
[4]*Department of Electrical and Computer Engineering, University of California Santa Barbara, Santa Barbara, California 93106, USA*
[5]*Center for High Technology Materials, University of New Mexico, 1313 Goddard St SE, Albuquerque, New Mexico 87106, USA*
*Corresponding author: heming.huang@telecom-paristech.fr

This work reports on a systematic investigation of the influence of optical feedback in InAs/GaAs quantum dot lasers epitaxially grown on silicon. The boundaries associated to the onset of the critical feedback level corresponding to the first Hopf bifurcation are extracted at different bias conditions with respect to the onset of the first excited state transition. Overall, results show that quantum dot lasers directly grown onto silicon are much more resistant to optical feedback than quantum well lasers, mostly resulting from a small linewidth enhancement factor of high-quality quantum dot material. However, results also unveil that the onset of the critical feedback level strongly depends on the excited-to-ground-state ratio, hence a figure of merit showing that a small ratio of the excited-to-ground-state lasing thresholds is not beneficial for maintaining a high degree of stability. This work brings further insights in the understanding of quantum dot laser physics and is useful for designing feedback resistant lasers for isolator-free transmission in metro, access, and data center optical networks, as well as for integrated photonics.   © 2018 Optical Society of America

OCIS codes: (140.5960) Semiconductor lasers; (250.0250) Optoelectronics; (190.3100) Instabilities and chaos.

https://doi.org/10.1364/JOSAB.35.002780

1. INTRODUCTION

Silicon photonics can provide novel functionality and high performance for applications in optical communications, sensing, and microelectronics. It is a serious candidate to replace electrical interconnects as transmission rates increase and lower energy consumption per bit becomes critically important [1,2]. Although silicon waveguides have low loss from 1 to 8 µm, the indirect bandgap nature of the silicon makes light emission inefficient and limits the applications of silicon photonics. To this end, on-chip light sources are usually engineered by depositing some other gain materials. For instance, significant breakthroughs have been achieved by integrating direct bandgap III–V compound semiconductors with silicon using flip-chip or wafer bonding [3,4]. While very good performance and complex integration have been reported, inexpensive and monolithically grown silicon light emitters with high yield and thermal stability are still desired. To achieve this goal, direct epitaxial growth of GaAs layers on silicon with InAs quantum dot (QD) nanostructures as a gain medium is a very

promising solution [5,6]. Because of the discrete energy levels, InAs/GaAs QDs have demonstrated for years their high potential for making optical transmitters with both high thermal stability and low threshold current density, which are in favor of reducing the energy per bit consumption [7]. Two research works revealed that QD lasers epitaxially grown on silicon exhibit relative intensity noise (RIN) from –140 to –150 dB/Hz, while that of QD lasers epitaxially on germanium is higher at –120 dB/Hz [8,9]. At the system level, an error-free transmission has been reported on a 12.5 Gbps directly modulated 1.3 µm InAs QD laser directly grown on silicon and with a power penalty less than 1 dB after a 12 km transmission distance at 5 Gbps [10]. As for the dynamic properties, QD lasers are richer compared to their quantum well (QW) counterparts, benefiting from the great competition between the quantum confined energy states [11,12]. Typically, QD lasers show three possible regimes of lasing operation, depending on the bias conditions: (i) ground state (GS) lasing, (ii) dual state emission showing an interplay dynamic between GS and the first excited

state (ES), and (iii) first ES lasing [13]. Under optical feedback, it was shown that while InAs/GaAs QD lasers emitting exclusively on the GS transition are much more stable, hence exhibiting chaos-free operation, those operating under the dual state lasing regime or on the sole ES transition can display a plethora of dynamic states, including chaotic states [14–17]. In the context of integrated photonics, investigating the effects of parasitic optical reflections on QD lasers grown either on silicon or germanium is of particular importance because no on-chip optical isolators integrated with lasers that have sufficient isolation ratio and low loss have yet been reported. Therefore, even a small backreflection from the optical fiber pigtail or optical connectors can highly degrade the laser performance [18,19]. Prior works have indeed already demonstrated that hybrid distributed feedback (DFB) semiconductor lasers heterogeneously integrated onto silicon are highly sensitive to intentional reflections originating from various possible interfaces (e.g., active and passive transition regrowth interfaces), hence making it necessary to include an expensive bulk isolator in the package [20,21]. More recently, the transition to the so-called coherence collapse regime, an unwanted feedback regime for high-speed data transmission, has been investigated in high coherence lasers made with hybrid silicon technology. Owing to the very large quality factor ($\approx 10^7$), the onset is found for about 20 dB higher reflection levels than in conventional semiconductor lasers [22]. As for lasers grown epitaxially on silicon, initial experiments have shown that silicon QD devices display a much better tolerance against optical perturbations. In particular, as compared to heterogeneously integrated QW lasers, a 20 dB reduced sensitivity to optical feedback is reported [23]. For industrial applications, the use of on-chip QD lasers without optical isolation could be envisioned for data transmission on a photonic integrated circuit as recently demonstrated [24,25]. The proposed module using a I/O core transmitter combined with external modulation can deliver error-free operation at a 25 Gbps data rate without optical isolation. In this paper, we go a step beyond by deeply analyzing the optical feedback dynamics in InAs/GaAs QD Fabry–Perot (FP) lasers epitaxially grown on silicon. The boundaries associated to the onset of critical feedback level corresponding to the first Hopf bifurcation are extracted at different bias conditions with respect to the onset of the first excited state transition. Overall, results show that QD lasers directly grown onto silicon are much more resistant to optical feedback, benefiting from a small linewidth enhancement factor (α_H-factor), a high size uniformity of nanostructures [26], and a large damping rate, as recently reported [10]. However, it is also unveiled that the onset of the critical feedback level strongly depends on the ES-to-GS lasing threshold ratio, meaning that the faster the switching to the ES, the stronger the sensitivity to the optical feedback. We believe that this work brings further insights in the understanding of QD laser physics and is useful for designing feedback resistant lasers for isolator-free transmission in metro, access, and data center optical networks, as well as for integrated photonics.

2. DESCRIPTION OF THE QUANTUM DOT LASERS

The QD lasers studied in this work are from the same bar, meaning that the gain medium is the same for all devices.
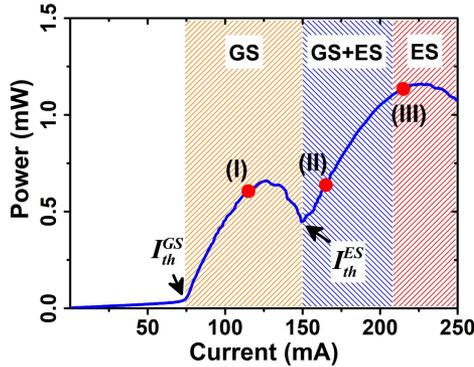
QD laser samples were grown in a Veeco Gen-II molecular beam epitaxy chamber. Figure 1 shows the QD laser structure epitaxially grown on an on-axis (001) GaP/Si wafer. Prior to the GaAs–AlGaAs graded-index separate confinement heterostructure, a 3 μm thick GaAs buffer layer was first grown to bridge the lattice mismatch to the Si wafer. The threading dislocation density (TDD) of the buffer layer was 3×10^8 cm^{-2} and QD density was 3×10^{10} cm^{-2}. Details on the epitaxial growth process can be found elsewhere [8]. The laser epitaxial material was processed to narrow ridge-waveguide lasers. Both n-type and p-type contact metals were formed on top of the etched mesa to avoid the GaAs and Si interface. After dicing and polishing the lasers, the facets of the 1 mm cavity were coated with 8 pairs and 1 pair of high-reflectivity (HR) films to achieve 95% and 55% reflectivity, respectively. Table 1 presents a list of the main parameters associated to the different QD devices, such as, from the left to the right, the ridge width, the threshold currents for each lasing state, namely, I_{th}^{GS} and I_{th}^{ES}, the ratio of the ES-to-GS lasing threshold ratio I_{th}^{ES}/I_{th}^{GS}, the peak wavelength for each lasing state, namely, $\lambda_{gainpeak}^{GS}$ and $\lambda_{gainpeak}^{ES}$, and the GS–ES energy separation. Although the devices exhibit a different ratio I_{th}^{ES}/I_{th}^{GS}, they all have a similar GS–ES separation of ~40 meV. Figure 2 displays the light-current (LI) characteristics of QD laser #4. The different regimes of operation discussed in the introduction can be identified with the two thresholds related to the GS and ES transitions, respectively. When the ES stimulated emission appears, a decrease of the GS slope efficiency is observed. Note that the red markers stand for bias levels used for optical spectra measurements, as shown in Fig. 3. At low bias, it is clear that the laser emits on the GS transition, then moves to the dual state lasing operation, and finally operates solely on the ES lasing state due to the GS quenching. From Table 1, QD laser samples can be categorized into two groups depending on their ES-to-GS lasing threshold ratio. QD lasers #1 and #2 have a large GS–ES contrast, while that of devices #3 and #4 is lower. This difference can be explained from the spectral-hole-burning-induced gain compression. Indeed, although the net gain at the GS is clamped at
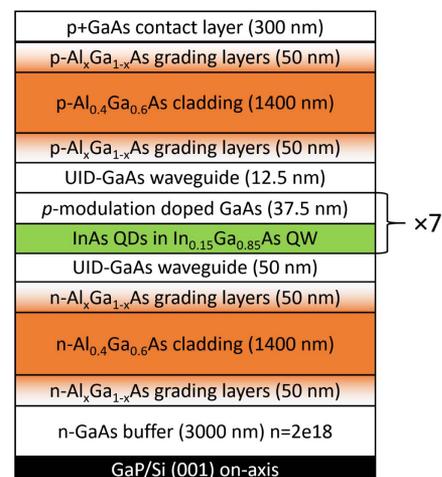
Fig. 1. Cross-sectional schematic of an InAs QD laser epitaxially grown on (001) GaP/Si.
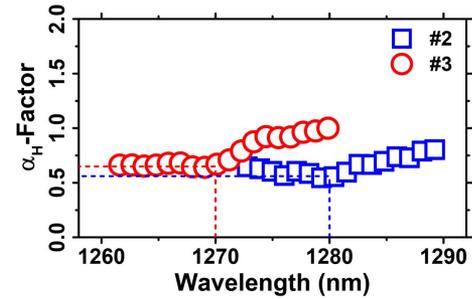
Table 1.   Parameters of the InAs/GaAs QD Lasers: Ridge Width, Threshold Currents, ES-to-GS Lasing Threshold Ratio, Peak Wavelengths, and GS–ES Energy Separation

Device	Ridge Width (μm)	I_{th}^{GS} (mA)	I_{th}^{ES} (mA)	I_{th}^{ES}/I_{th}^{GS}	$\lambda_{gainpeak}^{GS}$ (nm)	$\lambda_{gainpeak}^{ES}$ (nm)	GS–ES Separation (meV)
#1	3.5	46	261	5.7	~1280	~1230	~40
#2	3.5	50	274	5.5	~1280	~1230	~40
#3	3	63	169	2.7	~1270	~1220	~40
#4	3	74	149	2	~1270	~1220	~40

Fig. 2. Light-current characteristics of laser #4. The red markers correspond to the optical spectra depicted in Fig. 3.
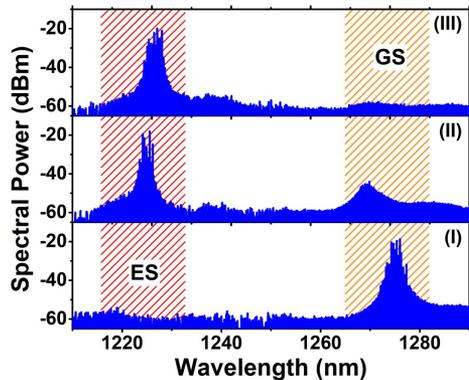
Fig. 3. Optical spectra measured for QD laser #4: (I) above the GS threshold, (II) near-above the ES threshold, and (III) well-above the ES threshold. The bias conditions correspond to the red markers reported in Fig. 2.

Fig. 4. Spectral dependence of the α_H-factor measured by ASE in QD lasers #2 and #3.

and in particular the influence of the ES. One parameter driving the optical feedback dynamics is the α_H-factor. In the specific case of QD lasers, it has been shown that a large inhomogeneous broadening and the presence of off-resonance lasing states contribute to enhance the effective α_H-factor measured above the laser's threshold [29,30]. As an example, the spectral dependence of the α_H-factor of QD lasers #2 and #3 are extracted from amplified spontaneous emission (ASE) in sub-threshold operation [31]. After a proper elimination of the thermal effects, Fig. 4 depicts values of about 0.55 and 0.65, respectively, at the gain peak, which are both smaller than those previously reported on InAs/GaAs QD lasers [32]. Such a low α_H-factor is an excellent prerequisite for improving the feedback resistance of QD lasers grown on silicon and results from the large QD size uniformity in the active region [2,26].

3. EXPERIMENTAL SETUP

Figure 5 depicts the setup used for the optical feedback experiments [32]. The emission from the laser diode at the 55% reflection front facet is coupled by anti-reflection (AR)-coated lens-end fiber and divided into two paths: a feedback path (90% of the coupled power) and a detection path (the remaining 10%). On the feedback path, a backreflector (BKR) is wired

threshold, the carrier density at the ES keeps growing due to spectral hole burning [27]. Thus, depending on the geometry of the waveguide, the gain compression effect is enhanced, leading to an effective gain compression coefficient, which can influence the onset of ES lasing. Also, it has to be noted that QD lasers with low GS threshold currents exhibit a better GS–ES contrast due to less thermal effects [28]. Possibly, Table 1 shows that the different threshold ratios of GS and ES can also be used as a hint for probing the different internal carrier dynamics among a set of QD lasers.
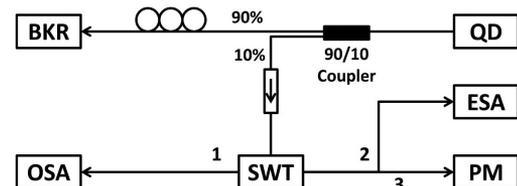
As all regimes of operation can be observed with those QD lasers, it is possible to track the sensitivity to optical feedback

Fig. 5. Experimental setup used for investigating optical feedback. QD, QD laser diode; BKR, backreflector; SWT, optical switch; OSA, optical spectrum analyzer; ESA, electrical spectrum analyzer; PM, powermeter.

to feed the light back to the laser cavity, forming a 7 m long fiberized external cavity. A polarization controller is then inserted to compensate for the fiber dispersion in the external cavity and to maximize the effects of the optical feedback, namely, to have the reflected light in the transverse electric (TE) polarization. The BKR, which consists of a mirror and a variable attenuator, is also used to control the feedback strength r_{ext}, defined as the ratio between the power return to the laser cavity and the laser free-space emitting power. The losses from the fiber coupling and in the fiber setup are taken into account to accurately calculate r_{ext}, for which the uncertainty is less than 0.1%. The remaining 10% of the coupled light from the laser device is sent on to the detection path and then isolated in order to prevent additional feedback from the connected equipment. An optical switch (SWT) is then implemented to swap the signal between the powermeter (PM) and the optical and electrical spectrum analyzers (OSAs and ESAs) for further analysis. In what follows, only the long delay regime is studied, meaning that the ratio between the frequency of the external cavity f_{ext} and the relaxation oscillation frequency f_{RO} is such that $f_{ext}/f_{RO} < 1$.

4. CRITICAL FEEDBACK LEVEL

Any semiconductor laser operating under external optical feedback can be described by a generalized complex electric field equation [33]:

$$\frac{dE}{dt} = \left[j(\omega - \omega_0) - \frac{j}{L} \int_{(L)} \frac{\partial W/\partial N}{\partial W/\partial \omega} \Delta N dz \right] E(t) - \frac{2C_k}{\tau_{in}} \sqrt{r_{ext}} E(t - \tau), \tag{1}$$

with ω and ω_0 as the lasing frequencies with and without the presence of optical feedback, respectively, τ the external round-trip time, L the laser cavity length, τ_{in} the photon round-trip time in the laser's cavity, and C_k the external coupling coefficient of the k-facet [$k = r, l$ for rear (r) or front (l)], whose general expression is given by [34]

$$C_k = \frac{j\tau_{in}}{2}(1 - r_k^2)\frac{\partial W/\partial r_k}{\partial W/\partial \omega}, \tag{2}$$

with r_k the amplitude reflectivity. W is the Wronskian operator, which, for a FP laser, is expressed as [34]

$$W = 2j\beta r_r(r_l r_e e^{-2j\beta L} - 1), \tag{3}$$

with β the complex propagation constant. The dependence of the Wronskian on the facet reflectivity is used to take into account external optical feedback coming from a distant reflecting point of amplitude reflectivity $\sqrt{r_{ext}}$ [in Eq. (1)]. Note that Eq. (1) extends the known Green's function approach to the case of external optical feedback and constitutes a sort of generalization of the Lang and Kobayashi rate equations, in which spatial hole burning effects are also included [35]. The dynamic evolution of the carrier density is then governed by the usual relation:

$$\frac{dN}{dt} = \frac{I}{e} - \frac{N}{\tau_c} - \frac{N}{\tau_{SRH}} - G|E|^2, \tag{4}$$

where N, τ_c, G, and I are the carrier density within the active zone, the carrier lifetime, the optical gain, and the injected

current, respectively. The lifetime τ_{SRH} is incorporated into the carrier equation to take into account the Shockley–Read–Hall (SRH) nonradiative recombinations induced by the epitaxial defects in QD lasers epitaxially grown on silicon. In what follows, the effective carrier lifetime is rewritten as

$$\tau_c'^{-1} = \tau_c^{-1} + \tau_{SRH}^{-1}. \tag{5}$$

From that, it turns out that epitaxial defects shorten the effective recombination lifetime, since the SRH contribution can be up to 10 ns in GaAs-based material systems, while it is less than 1 ns in Ge-based ones, for instance [36].

In this work, the optical feedback dynamic is analyzed through the prism of the critical feedback level r_{crit}, which corresponds to the birth of the laser destabilization associated to the first Hopf bifurcation [37]. Indeed, for semiconductor lasers operating under optical feedback, the undamping of the relaxation oscillations is a precursor of the quasi-periodicity route to chaotic oscillations through the fully developed coherence collapse regime [38], whose onset is often related to $r_{ext} = r_{crit}$ [39]. Using Eqs. (1) and (4) evaluated through small-signal analysis and assuming a long external cavity ($f_{ext}/f_{RO} < 1$), the onset of the critical level can be evaluated by the relationship

$$r_{crit} = \frac{\tau_{in}^2 (Af_{RO}^2 + 1/\tau_{c'})^2}{16C_l^2}\left(\frac{1 + \alpha_H^2}{\alpha_H^4}\right), \tag{6}$$

where A usually refers to the K-factor, an essential parameter driving the modulation capabilities of a semiconductor laser. Let us note that the K-factor is enhanced by the gain compression that is always larger in QD lasers [27]. Also, the K-factor strongly depends on the damping of the relaxation oscillations through the internal carrier timescales. For instance, assuming different electron–hole dynamics, it was shown that the relaxation oscillation frequency, the damping, and the modulation bandwidth of QD lasers are changed upon the electron scattering lifetime [40]. Using Eqs. (2) and (3) allows to us reduce the external coupling coefficient toward the external cavity to

$$C_l = \frac{1 - r_l^2}{2r_l}. \tag{7}$$

Practically, Eq. (6) gives the maximum parasitic feedback ratio that can be tolerated for stable operation of the laser into a communications system. As the relaxation oscillation frequency scales up with the bias current, the critical feedback level is expected to rise accordingly. To this end, feedback resistant lasers can be made in particular by minimizing the α_H-factor, which means that results depicted in Fig. 4 are an excellent prerequisite to reaching this goal. Another possibility is to consider a very long cavity with low loss in order to combine a high quality factor with a low C_l coefficient, but doing so is not always desired for high-speed direct modulation for which a large relaxation oscillation frequency is desired [10,22,41].

Figure 6 gives the computed values of the critical feedback level as a function of the α_H-factor for different τ_{SRH} of 0.1, 0.5, 1, and 5 ns. Although the SRH is also expected to slightly affect the α_H-factor, it is assumed here that the dominant contribution of such nonradiative contributions in Eq. (6) remains on the damping factor $A \times f_{RO}^2 + 1/\tau_c'$. Parameters used for the simulations are $\tau_{in} = 23$ ps, $f_r = 3$ GHz, $A = 1$ ns,
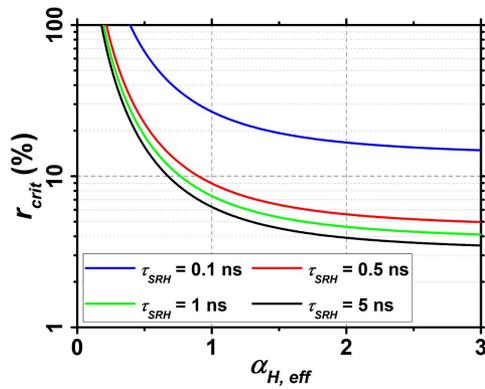
Fig. 6. Critical feedback level r_{crit} as a function of the effective α_H-factor for $\tau_{SRH} = 0.1$, 0.5, 1, and 5 ns, according to Eq. (6).
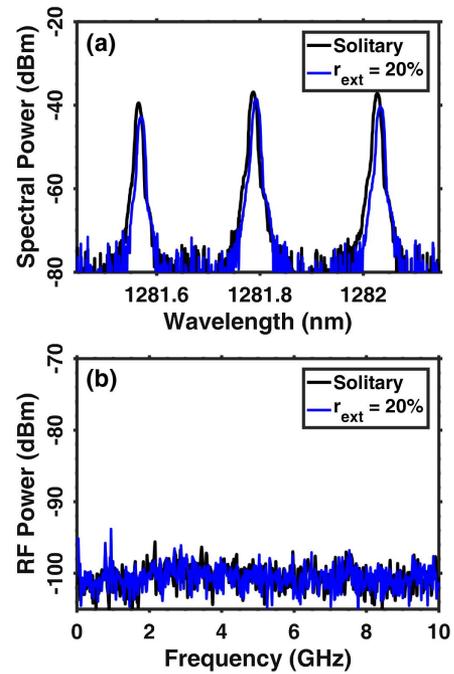
$C_l = 0.3$, and $\tau_c = 1.5$ ns [23]. As the pump current and the temperature are fixed, both the relaxation oscillation frequency and the K-factor used in these simulations can be considered constants. As for the latter, a value of about 1 ns has been recently reported up to $8 \times I_{th}$ on other samples made with similar gain media [10]. Last but not least, it has to be noted that the simulations are conducted above threshold, meaning that α_H should be most likely considered as an effective parameter for QD lasers strongly influenced by nonlinear gain effects and off-resonance lasing states [26,30]. Figure 6 shows that the critical feedback level is strongly affected by the SRH recombinations. Hence, for $\alpha_H < 1$, the onset of the instabilities is up-shifted by several orders of magnitude. For instance, for $\alpha_H = 1$, r_{crit} increases from 6% to about 27% when the SRH recombination lifetime is shortened. In other words, the QD oscillator becomes so overdamped for higher TDD and epitaxial defects that the feedback sensitivity is drastically reduced.

5. RESULTS AND DISCUSSION

In this section, the optical feedback dynamics with respect to the critical level is studied. The influence of the ES is also discussed for all lasers.

A. Maximum Optical Feedback Tolerance

To start with, let us investigate the optical feedback dynamics of a QD laser having a high GS–ES contrast. Figure 7 depicts the optical and radio frequency (RF) spectra of QD laser #2 in free-running condition $r_{ext} = 0$ (black ones) and under $r_{ext} = 20\%$ optical feedback (blue ones) at a bias condition of $2 \times I_{th}$. At this bias level, the laser emits before the occurrence of the ES. As noted, even at a very high value of r_{ext}, the laser stability is maintained. Apart from a slight wavelength shift, no sign of distortion is observed on the FP modes, and the corresponding RF spectrum remains flat without any visible periodic or chaotic oscillations. The QD laser is shown in this case quasi-insensitive to optical feedback, taking into account the fact that 20% of light reinjected into the laser is already much larger than any typical reflection levels taking place in a transmission system. Such feedback resistance up to 20% is higher than the tolerance level previously reported in GaAs-based QD lasers [42,43], and is very promising for the conception of

isolator-free on-chip optical transmitters. To illustrate the feedback sensitivity of QD laser with a low GS–ES contrast, Fig. 8 represents the optical and RF spectra taken at $2 \times I_{th}$, i.e., the same bias level as for QD laser #2, namely, below the onset of the ES transition. Compared to Fig. 7, the behavior of this laser

Fig. 7. (a) Optical and (b) RF spectra for QD laser #2 operating in the free-running $r_{ext} = 0$ (black) condition and under $r_{ext} = 20\%$ optical feedback at $2 \times I_{th}$.
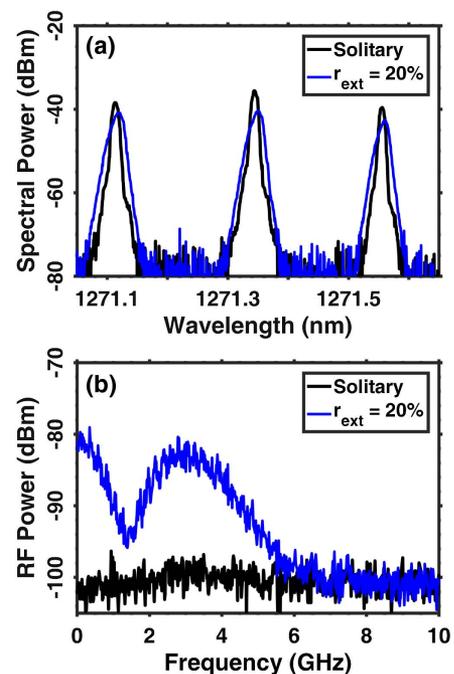

Fig. 8. (a) Optical and (b) RF spectra for QD laser #3 operating in the free-running (black) condition and under $r_{ext} = 20\%$ optical feedback at $2 \times I_{th}$.

is fundamentally different. Without optical feedback, the longitudinal FP modes are not altered. However, at high feedback strength ($r_{ext} = 20\%$), the FP modes are significantly broadened, which is the signature of a chaotic behavior as confirmed by the broadband RF spectrum. The low-frequency part below 2 GHz is attributed to partition noise coming from the multimode behavior, whereas beyond, the magnitude of the chaotic bandwidth is driven mostly by the relaxation oscillation frequency [37]. As a conclusion, although the QD lasers share the same gain medium, it turns out that the responses to optical feedback are different. As will be discussed in what follows, this difference is attributed to the ES-to-GS threshold ratio and how fast the ES switching dynamics takes place with respect to the bias current operation.

B. Dynamical Routes

To clarify the optical feedback dynamics of QD laser #3, Fig. 9 shows the optical and RF mapping spectra as a function of the feedback strength r_{ext} ranging from 0% to 15%. The first column depicts the evolution of the gain peak longitudinal mode, whereas the second shows the dynamical route in the RF domain. To cover the different regimes of operation, three different bias currents are considered: 2×, 2.85×, and $3.75 \times I_{th}^{GS}$. First, Fig. 9(e) shows that the modal broadening corresponding to the critical feedback level takes place at $r_{ext} = 5.6\%$, which is slightly different than what is observed in Fig. 9(f), in which the destabilization appears at $r_{ext} = 7\%$. Such difference can be due to the detection path, from which only 10% of the lasing beam is coupled into the optical fiber; therefore, the amount of optical power transmitted to the spectral analyzers is weaker.
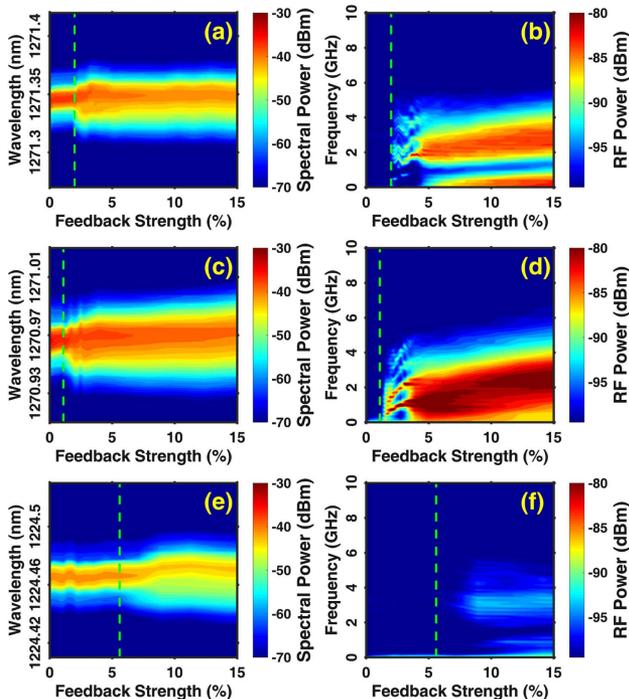

Fig. 9. Optical (first column) and RF (second column) spectra mappings of QD laser #3 measured at (a),(b) 2×, (c),(d) 2.85×, and (e),(f) $3.75 \times I_{th}^{GS}$ bias. The green lines mark the critical feedback levels.

Thus, extracting the critical feedback level r_{crit} from the green vertical dashed lines through the optical spectral maps in Figs. 9(a), 9(c), and 9(e) allow us to locate the critical levels for QD laser #3 at 2%, 1%, and 5.6%, respectively. These results indicate that once the ES transition has passed, the resistance to optical feedback has increased. In other words, while approaching the GS–ES dual state lasing regime, the laser stability originally emitting on the GS is affected. In this interplay regime where the laser moves from the GS to the ES, a route to chaos with higher complexity is observed as compared to the feedback-induced dynamics from the sole lasing state operation.

C. Impact of the ES Transition

To verify the previous assumptions, similar measurements are now performed on the other devices with respect to bias level. Figure 10 depicts the extracted r_{crit} as a function of the bias level normalized to the ES threshold current I/I_{th}^{ES} for QD lasers #1, #2, #3, and #4. Overall, the same behavior is observed, hence the evolution of r_{crit} strongly depends on the ES-to-GS threshold ratio. For $I/I_{th}^{ES} < 1$, the laser exhibits its higher resistance to optical feedback at low biases because only GS lasing occurs. As the bias current increases, the critical feedback level decreases due to the progressive occurrence of the ES. For instance, in case of QD laser #1, r_{crit} collapses from 12% down to 2.5%. Note that the decrease of the critical feedback level with the bias current is in agreement with a prior work performed on InAs/GaAs QD lasers [32,44]. Surprisingly, once the ES emission occurs ($I/I_{th}^{ES} > 1$), Fig. 10 shows a change in the laser dynamics, since the critical feedback level re-increases with the bias current as for single-mode lasers and contributes somewhat to restabilizing the laser. Figure 10 also confirms from the black arrow that a large ratio I_{th}^{ES}/I_{th}^{GS} increases the laser stability. For instance, at $0.7 \times I_{th}^{ES}$, the values for r_{crit} between QD lasers #1 and #4 differ by a factor of 60, namely, they are, respectively, 6% and 0.1%. In the ultimate case for which the QD laser remains on GS transition whatever the bias current ($I_{th}^{ES}/I_{th}^{GS} \rightarrow \infty$), a high stability associated to a chaos-free operation can possibly be observed, as recently unveiled with QD lasers on native GaAs substrate [14]. Overall, these different observed dynamics are most likely due to the carrier filling in the ES, which balloons the α_H associated to the GS transition, leading to a reduction of the critical feedback level [30,45]. Then, once the laser operates on the sole ES, the differential gain becomes larger, hence re-increasing the critical feedback level through a reduction of the α_H associated to the ES transition [4,13,46]. In addition, it is important to stress that, once the laser is on the sole ES transition, any further increase of the pump current also raises the damping accordingly, resulting in the restabilization of the lasers against optical feedback [47,48]. Although such a higher feedback resistance should also slow down the modulation dynamics, it has been shown that the ES QD laser can, however, exhibit faster speed under direct modulation owing to larger differential gain and less gain nonlinearities [13]. Last but not least, QD lasers with smaller I_{th}^{ES}/I_{th}^{GS} ratio have a higher ES differential gain [49], results depicted in Fig. 10 also prove that they are more easily perturbed by unwanted reflections.
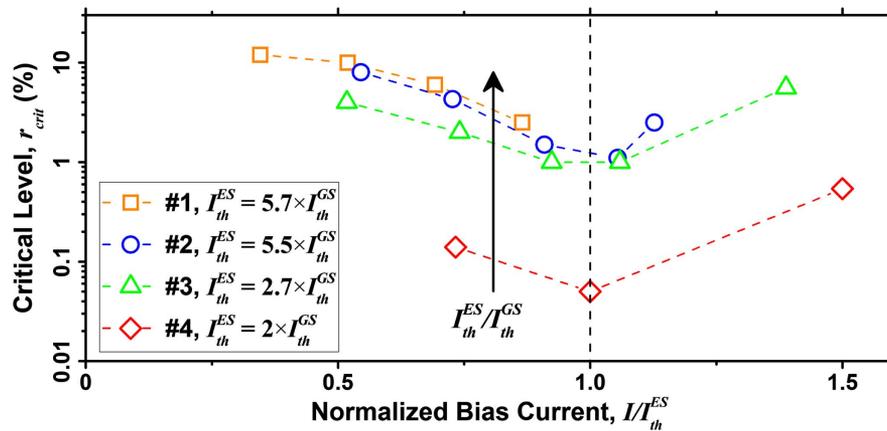
Fig. 10. Critical feedback level r_{crit} for QD lasers #1, #2, #3, and #4 (with different ratio $I_{\text{th}}^{\text{ES}}/I_{\text{th}}^{\text{GS}}$) plotted as a function of the ratio of the bias current to the ES lasing threshold $I/I_{\text{th}}^{\text{ES}}$.

6. CONCLUSIONS

In this work, we have investigated the optical feedback dynamics of QD lasers epitaxially grown on silicon. Results have shown that such lasers are highly stable under optical feedback owing to the small α_H factor, the low QD size inhomogeneity, and the large damping rate [10,26]. On the other hand, our results also prove that the critical feedback level strongly depends on the ES-to-GS, lasing threshold ratio, which can be considered as an additional figure of merit of the feedback dynamics, thus a laser having a fast switching dynamics with respect to the bias current is more subject to being highly destabilized by parasitic reflections. However, at this stage, it is clear that further investigation on the influence of the SRH recombinations on the damping factor, the α_H, and the feedback sensitivity of a low TDD QD laser needs to be performed [50]. To sum, this work brings novel insights in the understanding of QD laser physics that are useful for designing feedback resistant lasers in compliance with both short- and long-haul communication links. The next step will also involve numerical modeling of QD lasers epitaxially grown on silicon, including the SRH contribution, as well as performing further optical feedback experiments so as to locate more complex dynamics in particular within the short cavity regime [8,14,51].

REFERENCES

1. R. Stabile, A. Albores-Mejia, A. Rohit, and K. A. Williams, "Integrated optical switch matrices for packet data networks," Microsyst. Nanoeng. **2**, 15042 (2016).
2. J. C. Norman, D. Jung, Y. Wan, and J. E. Bowers, "Perspective: the future of quantum dot photonic integrated circuits," APL Photon. **3**, 030901 (2018).
3. G. Roelkens, L. Liu, D. Liang, R. Jones, A. Fang, B. Koch, and J. Bowers, "III-V/silicon photonics for on-chip and intra-chip optical interconnects," Laser Photon. Rev. **4**, 751–779 (2010).
4. T. Katsuaki, W. Katsuyuki, and Y. Arakawa, "III-V/Si hybrid photonic devices by direct fusion bonding," Sci. Rep. **2**, 349 (2012).
5. J. Norman, M. J. Kennedy, J. Selvidge, Q. Li, Y. Wan, A. Y. Liu, P. G. Callahan, M. P. Echlin, T. M. Pollock, K. M. Lau, A. C. Gossard, and J. E. Bowers, "Electrically pumped continuous wave quantum dot lasers epitaxially grown on patterned, on-axis (001) Si," Opt. Express **25**, 3927–3934 (2017).
6. S. Chen, W. Li, J. Wu, Q. Jiang, M. Tang, S. Shutts, S. N. Elliott, A. Sobiesierski, A. J. Seeds, I. Ross, P. M. Smowton, and H. Liu, "Electrically pumped continuous-wave III-V quantum dot lasers on silicon," Nat. Photonics **10**, 307–311 (2016).
7. G. Eisenstein and D. Bimberg, *Green Photonics and Electronics* (Springer, 2017).
8. A. Y. Liu, J. Peters, X. Huang, D. Jung, J. Norman, M. L. Lee, A. C. Gossard, and J. E. Bowers, "Electrically pumped continuous-wave 1.3 μm quantum-dot lasers epitaxially grown on on-axis (001) GaP/Si," Opt. Lett. **42**, 338–341 (2017).
9. Y.-G. Zhou, C. Zhou, C.-F. Cao, J.-B. Du, Q. Gong, and C. Wang, "Relative intensity noise of InAs quantum dot lasers epitaxially grown on Ge," Opt. Express **25**, 28817 (2017).
10. D. Inoue, D. Jung, J. Norman, Y. Wan, N. Nishiyama, S. Arai, A. C. Gossard, and J. E. Bowers, "Directly modulated 13 μm quantum dot lasers epitaxially grown on silicon," Opt. Express **26**, 7022 (2018).
11. M. Virte, S. Breuer, M. Sciamanna, and K. Panajotov, "Switching between ground and excited states by optical feedback in a quantum dot laser diode," Appl. Phys. Lett. **105**, 121109 (2014).
12. E. A. Viktorov, P. Mandel, I. O'Driscoll, O. Carroll, G. Huyet, J. Houlihan, and Y. Tanguy, "Low-frequency fluctuations in two-state quantum dot lasers," Opt. Lett. **31**, 2302–2304 (2006).
13. D. Arsenijević, A. Schliwa, H. Schmeckebier, M. Stubenrauch, M. Spiegelberg, D. Bimberg, V. Mikhelashvili, and G. Eisenstein, "Comparison of dynamic properties of ground- and excited-state emission in p-doped InAs/GaAs quantum-dot lasers," Appl. Phys. Lett. **104**, 181101 (2014).
14. H. Huang, L.-C. Lin, C.-Y. Chen, D. Arsenijević, D. Bimberg, F.-Y. Lin, and F. Grillot, "Multimode optical feedback dynamics in InAs/GaAs quantum dot lasers emitting exclusively on ground or excited states: transition from short- to long-delay regimes," Opt. Express **26**, 1743–1751 (2018).
15. L.-C. Lin, C.-Y. Chen, H. Huang, D. Arsenijević, D. Bimberg, F. Grillot, and F.-Y. Lin, "Comparison of optical feedback dynamics of InAs/GaAs quantum-dot lasers emitting solely on ground or excited states," Opt. Lett. **43**, 210–213 (2018).
16. K. Lüdge, *Nonlinear Laser Dynamics: from Quantum Dots to Cryptography* (Wiley, 2012).

17. R. Pawlus, S. Breuer, and M. Virte, "Relative intensity noise reduction in a dual-state quantum-dot laser by optical feedback," Opt. Lett. **42**, 4259–4262 (2017).

18. R. B. Clarke, "The effect of reflections on the system performances of intensity modulated laser diodes," IEEE J. Lightwave Technol. **9**, 741–749 (1991).

19. F. Grillot, B. Thedrez, J. Py, O. Gauthier-Lafaye, V. Voiriot, and J. Lafragette, "2.5 Gb/s transmission characteristics of 1.3-μm DFB lasers with external optical feedback," IEEE Photon. Technol. Lett. **14**, 101–103 (2002).

20. K. Schires, N. Girard, G. Baili, G. H. Duan, S. Gomez, and F. Grillot, "Dynamics of hybrid III–V silicon semiconductor lasers for integrated photonics," IEEE J. Sel. Top. Quantum Electron. **22**, 43–49 (2016).

21. K. Schires, S. Gomez, A. Gallet, G. H. Duan, and F. Grillot, "Passive chaos bandwidth enhancement under dual-optical feedback with hybrid III-V/Si DFB laser," IEEE J. Sel. Top. Quantum Electron. **23**, 1–9 (2017).

22. M. Harfouche, "The coherence collapse regime of high-coherence Si/III-V lasers and the use of swept frequency semiconductor lasers for full field 3D imaging," Ph.D. thesis (California Institute of Technology, 2018).

23. A. Y. Liu, T. Komljenovic, M. L. Davenport, A. C. Gossard, and J. E. Bowers, "Reflection sensitivity of 1.3 μm quantum dot lasers epitaxially grown on silicon," Opt. Express **25**, 9535–9543 (2017).

24. K. Mizutani, K. Yashiki, M. Kurihara, Y. Suzuki, Y. Hagihara, N. Hatori, T. Shimizu, Y. Urino, T. Nakamura, K. Kurata, and Y. Arakawa, "Isolator free optical I/O core transmitter by using quantum dot laser," in *IEEE 12th International Conference on Group IV Photonics (GFP)* (2015), pp. 177–178.

25. K. Yashiki, K. Mizutani, J. Ushida, Y. Suzuki, M. Kurihara, M. Tokushima, J. Fujikata, Y. Hagihara, and K. Kurata, "25-Gbps error-free operation of chip-scale Si-photonics optical transmitter over 70°C with integrated quantum dot laser," in *Optical Fiber Communication Conference* (Optical Society of America, 2016), paper Th1F.7.

26. J. Duan, H. Huang, D. Jung, Z. Zhang, J. Norman, J. E. Bowers, and F. Grillot, "Semiconductor quantum dot lasers epitaxially grown on silicon with low linewidth enhancement factor," Appl. Phys. Lett. **112**, 251111 (2018).

27. F. Grillot, B. Dagens, J. Guy Provost, H. Su, and L. F. Lester, "Gain compression and above-threshold linewidth enhancement factor in 1.3-μm InAs-GaAs quantum-dot lasers," IEEE J. Quantum Electron. **44**, 946–951 (2008).

28. M. Gioannini, "Ground-state power quenching in two-state lasing quantum dot lasers," J. Appl. Phys. **111**, 043108 (2012).

29. C. Wang, M. Osinski, J. Even, and F. Grillot, "Phase-amplitude coupling characteristics in directly modulated quantum dot lasers," Appl. Phys. Lett. **105**, 221114 (2014).

30. F. Grillot, B. Dagens, J. G. Provost, H. Su, and L. F. Lester, "Gain compression and above-threshold linewidth enhancement factor in 1.3-μm InAs-GaAs quantum-dot lasers," IEEE J. Quantum Electron. **44**, 946–951 (2008).

31. C. Wang, K. Schires, M. Osiński, P. J. Poole, and F. Grillot, "Thermally insensitive determination of the linewidth broadening factor in nano-structured semiconductor lasers using optical injection locking," Sci. Rep. **6**, 27825 (2016).

32. H. Huang, H. Arsenijević, K. Schires, T. Sadeev, D. Bimberg, and F. Grillot, "Multimode optical feedback dynamics of InAs/GaAs quantum-dot lasers emitting on different lasing states," AIP Adv. **6**, 125114 (2016).

33. F. Grillot, G. H. Duan, and B. Thedrez, "Feedback sensitivity and coherence collapse threshold of semiconductor DFB lasers with complex structures," IEEE J. Quantum Electron. **40**, 231–240 (2004).

34. F. Grillot, "On the effects of an antireflection coating impairment on the sensitivity to optical feedback of AR/HR semiconductor DFB lasers," IEEE J. Quantum Electron. **45**, 720–729 (2009).

35. R. Lang and K. Kobayashi, "External optical feedback effects on semiconductor injection laser properties," IEEE J. Quantum Electron. **16**, 347–355 (1980).

36. K. Sears, M. Buda, H. H. Tan, and C. Jagadish, "Modeling and characterization of quantum dot lasers grown using metal organic chemical vapor deposition," J. Appl. Phys. **101**, 013112 (2007).

37. A. Uchida, *Optical Communication with Chaotic Lasers: Applications of Nonlinear Dynamics and Synchronization* (Wiley, 2012).

38. D. Lenstra, B. Verbeek, and A. D. Boef, "Coherence collapse in single-mode semiconductor lasers due to optical feedback," IEEE J. Quantum Electron. **21**, 674–679 (1985).

39. Q. Zou and S. Azouigui, "Analysis of coherence-collapse regime of semiconductor lasers under external optical feedback by perturbation method," in *Semiconductor Laser Diode*, D. Patil, ed. (InTech, 2012), Chap. 5.

40. B. Lingnau, K. Lüdge, W. W. Chow, and E. Schöll, "Influencing modulation properties of quantum-dot semiconductor lasers by carrier lifetime engineering," Appl. Phys. Lett. **101**, 131107 (2012).

41. C. T. Santis, S. T. Steger, Y. Vilenchik, A. Vasilyev, and A. Yariv, "High-coherence semiconductor lasers based on integral high-Q resonators in hybrid Si/III-V platforms," Proc. Natl. Acad. Sci. USA **111**, 2879–2884 (2014).

42. D. O'Brien, S. Hegarty, G. Huyet, J. McInerney, T. Kettler, M. Laemmlin, D. Bimberg, V. Ustinov, A. Zhukov, S. Mikhrin, and A. Kovsh, "Feedback sensitivity of 1.3 μm InAs/GaAs quantum dot lasers," Electron. Lett. **39**, 1819 (2003).

43. H. Huang, K. Schires, L.-C. Lin, C.-Y. Chen, D. Arsenijević, D. Bimberg, F.-Y. Lin, and F. Grillot, "Dynamics of excited-state InAs/GaAs Fabry-Perot quantum-dot lasers under optical feedback," in *Conference on Lasers and Electro-Optics* (Optical Society of America, 2016), paper STh4L.6.

44. F. Grillot, N. A. Naderi, M. Pochet, C.-Y. Lin, and L. F. Lester, "Variation of the feedback sensitivity in a 1.55 μm InAs/InP quantum-dash Fabry-Perot semiconductor laser," Appl. Phys. Lett. **93**, 191108 (2008).

45. S. Melnik, G. Huyet, and A. V. Uskov, "The linewidth enhancement factor α of quantum dot semiconductor lasers," Opt. Express **14**, 2950–2955 (2006).

46. R. Heitz, A. Kalburge, Q. Xie, M. Grundmann, P. Chen, A. Hoffmann, A. Madhukar, and D. Bimberg, "Excited states and energy relaxation in stacked InAs/GaAs quantum dots," Phys. Rev. B **57**, 9050–9060 (1998).

47. J. Mørk, B. Tromborg, and J. Mark, "Chaos in semiconductor lasers with optical feedback: theory and experiment," IEEE J. Quantum Electron. **28**, 93–108 (1992).

48. C. Otto, B. Globisch, K. Lüdge, E. Schöll, and T. Erneux, "Complex dynamics of semiconductor quantum dot lasers subject to delayed optical feedback," Int. J. Bifur. Chaos **22**, 1250246 (2012).

49. Q. Cao, S. F. Yoon, C. Z. Tong, C. Y. Ngo, C. Y. Liu, R. Wang, and H. X. Zhao, "Two-state competition in 1.3 μm multilayer InAs/InGaAs quantum dot lasers," Appl. Phys. Lett. **95**, 191101 (2009).

50. D. Jung, J. Norman, M. J. Kennedy, C. Shang, B. Shin, Y. Wan, A. C. Gossard, and J. E. Bowers, "High efficiency low threshold current 1.3 μm InAs quantum dot lasers on on-axis (001) GaP/Si," Appl. Phys. Lett. **111**, 122107 (2017).

51. T. Heil, I. Fischer, W. Elsäßer, and A. Gavrielides, "Dynamics of semiconductor lasers subject to delayed optical feedback: the short cavity regime," Phys. Rev. Lett. **87**, 243901 (2001).